# Confinement-Sensitive Optical Response of Cholesteric Liquid Crystals in Electrospun Fibers

**Eva Enz,[†] Vera La Ferrara,[‡] and Giusy Scalia[§,*]**

[†]Institut für Chemie-Physikalische Chemie, Martin-Luther-Universität Halle-Wittenberg, von-Danckelmann-Platz 4, 06120 Halle, Germany, [‡]ENEA C.R. Portici, P.le E. Fermi, Portici, Italy, and [§]Graduate School of Convergence Science & Technology, and Advanced Institutes of Convergence Technology, Seoul National University, 443-270 Suwon, Korea

**ABSTRACT** Soft self-assembling photonic materials such as cholesteric liquid crystals are attractive due to their multiple unique and useful properties, in particular, an optical band gap that can be continuously and dynamically tuned in response to weak external influences, easy device integration, compatibility with flexible architectures, and, as shown here, potential for submicrometer optical applications. We study such a system formed by a short-pitch cholesteric confined in the core of polymer fibers produced by coaxial electrospinning, showing that the selective reflection arising from the helical photonic structure of the liquid crystal is present even when its confining cavity is well below a micrometer in thickness, allowing as little as just half a turn of the helix to develop. At this scale, small height variations result in a dramatic change in the reflected color, in striking difference to the bulk behavior. These conclusions are made possible by combining focused ion beam (FIB) dissection and imaging of the internal fiber morphology with optical microscopy. The FIB dissection further reveals that the cross section of the cavity within the fiber can have a shape that is quite different from that of the outside fiber. This is critical for the photonic behavior of the composite fiber because different optical textures are generated not only by change in thickness but also by the shape of the cavity. Our results provide insights into the behavior of cholesterics in submicrometer cavities and demonstrate their potential at such dimensions.

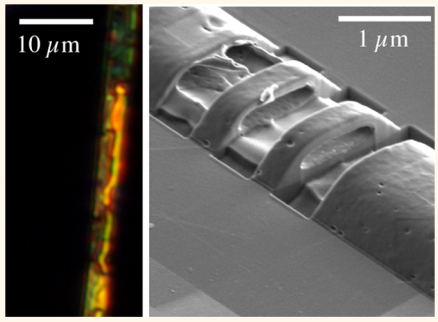


**KEYWORDS:** submicrometer confinement · photonic crystal · cholesteric liquid crystal · electrospun composite fibers · focused ion beam

The creation of new engineered materials *via* periodic or aperiodic nanostructures, not present in nature, allows the realization of unconventional and novel optical effects like negative refraction, thus paving the way to groundbreaking new applications.[1,2] Attention is now drawn toward reconfigurable and switchable systems to add dynamic modulation of light.[3,4] In this respect, soft materials with self-assembled ordered structures are particularly attractive because of their static and dynamic tunability, ease of integration in micro- and nanophotonic systems, and their compatibility with flexible substrates useful in, for example, wearable technology or biomedical applications.[5−16]

Short-pitch cholesteric liquid crystals are an intriguing example of soft materials with attractive photonic properties arising from self-organization on two different scales.[17] On the nanoscale, the molecules (typically rod-shaped) align along a common direction termed the director **n**, and on a supramolecular scale, **n** is then modulated in a helical fashion along a direction **k**⊥**n**, with periodicity (pitch) $p$ which is on the order of light wavelengths. This modulation renders cholesterics self-assembled photonic crystals with iridescent reflection within a narrow band gap centered at a wavelength $\lambda = pn_a$, where $n_a$ is the average refractive index of the cholesteric. For these wavelengths, the helical structure, moreover, introduces a polarization selectivity, such that only circularly polarized light with the same handedness as the helix is blocked from transmission through the cholesteric and instead reflected, while the opposite handedness passes unobstructed. A cholesteric sample illuminated by unpolarized white light therefore reflects strongly colored light that is circularly polarized with the same handedness as the liquid crystal helix. This phenomenon, known as

* Address correspondence to giusy.scalia@solcanta.com.

Received for review January 6, 2013 and accepted July 4, 2013.

**Published online July 04, 2013**
**10.1021/nn400066n**

selective reflection, is quite unique and interesting since colors are generated not by selective light absorption by dyes but by the helical structure and fine-tuned *via* the pitch length.[18] The softness of the liquid crystal phase furthermore makes it highly responsive to external stimuli like temperature variation, field application, gas diffusion, or mechanical stresses, all of which can influence the helix pitch. Accordingly, the reflection wavelength changes strongly as a result of subtle changes in the environment of the cholesteric, opening for innovative uses, for example, in autonomous gas sensors[19] or as tunable omnidirectionally lasing microdroplets.[20]

The self-organization of cholesterics provides the great practical advantage of making complex manufacturing processes unnecessary. In fact, the helical arrangement is spontaneously and easily formed, avoiding sophisticated and long lithographic steps typical of top-down approaches. This, in combination with the unique optical properties that result from the helical structure and the consequent rich application potential described above, makes it very attractive to integrate cholesterics into metamaterials or optical circuits. Examples of the beneficial integration of liquid crystals into microphotonic structures can be found, for example, in work on photonic crystal fibers[21] or related structures based on regular micropore arrangements. By infiltrating the pores with liquid crystal, the periodic refractive index modulation can conveniently be tuned. Mertens *et al.* demonstrated a temperature-controlled spectral shift of the defect mode in a silicon-based 3D photonic crystal infiltrated by a nonchiral nematic,[22] and Takeda and Yoshino predicted dynamic control of light propagation in a 2D photonic crystal following the same principles.[23]

The alignment and arrangement of liquid crystal molecules in confined structures is, however, not obvious, and it depends on several factors, such as surface interactions, cavity dimensions, and, in the case of cholesterics, the helix pitch. In ref 24, cholesteric liquid crystals were infiltrated in submicrometer cylindrical cavities of alumina membranes and the molecular orientation within the pores was derived from $^2$H NMR. Depending on the pitch, a transition from a radially to an axially twisted structure occurred. Director profiles of cholesterics in glass capillaries ranging from 25 to 200 $\mu$m in diameter were systematically studied by Kitzerow *et al.* as function of the liquid crystal pitch, tuned by temperature, for parallel and perpendicular anchoring with respect to the surfaces.[25] The authors found that the liquid crystal alignment depends on the ratio of the diameter of the cylindrical capillaries and the pitch, with several interesting structures and defect arrangements being observed. The effect of changing the channel diameter was further investigated by Matthias *et al.*[26] Using short- and long-pitch cholesterics, the authors evaluated experimentally and modeled theoretically the profile of the liquid crystal director in macropores of silicon photonic crystals. Again, the cavity dimensions, the pitch, and their ratio influence the liquid crystal organization.

In the present study, we realize submicrometer confinement of short-pitch cholesterics by electrospinning the liquid crystal coaxially inside a polymer solution, resulting in a novel type of core–sheath photonic microfiber. Our approach differs from previous work in terms of material, production technique, as well as scale. To the best of our knowledge, the produced fibers constitute the first case of submicrometer confinement in an optically transparent long channel. Our detailed investigation is motivated by a recent optical microscopy study, in which it was qualitatively confirmed that the attractive optical properties of cholesterics are largely preserved even under such strong confinement.[27] However, since the specific optical behavior is expected to be dependent on the dimension[26] and shape of the cavity containing the liquid crystal, and since it has been theoretically predicted that the reflectivity decreases, exhibiting a broader response of the reflected wavelength as the number of pitches fitting in the cavity is diminished,[28] it is of crucial importance to correlate the optical signature with the internal structure at submicrometer scale. Such an investigation has not yet been reported.

We study the internal structure of electrospun cholesteric liquid crystal-functionalized fibers by sectioning them along specific patterns with focused ion beam (FIB), and we correlate the revealed cavities with the observed optical microscopy texture. The cavities are found to be in the submicrometer range at least in one dimension, fitting only very few pitch lengths of the cholesteric helix. We find that at this scale a small variation of the cavity height produces strong changes in the reflected colors. Moreover, we show that even when just one-half turn of the cholesteric helix fits in the cavity, colorful reflection can still be observed. Our observations constitute a striking demonstration of the benefit of helical arrangements for photonics, as the periodicity is inherent at any scale in this fully continuous structure, in stark contrast to layered and thus discrete photonic crystals.

## RESULTS AND DISCUSSION

**Coaxial Electrospinning.** Our functional composite fibers, which are produced by coaxial electrospinning of the liquid crystal as a core fluid inside a sheath fluid such as polyvinylpyrrolidone (PVP) in ethanol,[27,29,30] alternatively employing phase separation between liquid crystal and polymer,[31] constitute a new class of innovative polymer composites. In such fibers, as confirmed by polarized Raman scattering[30] as well as X-ray scattering,[29] the liquid crystal aligns planarly at the interface with the polymer sheath, with **n** along the fiber axis. This direction of alignment can be explained

as a result of the PVP chains being aligned by stretching during the spinning process, giving a similar director templating effect as for rubbed polymer alignment layers in standard cells. The helix of an encapsulated cholesteric thus develops perpendicular to the fiber, allowing the selective reflection to be seen from the composite fiber.[27]

Coaxial electrospinning is a versatile technique for producing functional composite fibers of various types and thickness down to a few tens of nanometers, and the interest in the technique has been strongly rising in recent years.[30,32−36] It is attractive also for photonics since the produced fibers can exhibit a variety of useful optical properties.[29,37,38] For characterizing the core−sheath structure, a commonly employed approach is to carry out scanning electron microscopy (SEM) on the fractured end surface of fibers that have been broken into two sections.[39] The method, however, requires a fiber sheath that is brittle enough for the morphology to stay intact upon fracture, a requirement that is not met by the fibers studied here. The rather soft PVP sheath collapses upon fracturing, closing up the core entirely and thus blocking the view of the fiber interior. Moreover, the method does not let the user choose the location of the fracture, nor does it allow longitudinal sectioning. One can thus not be certain that the particular imaged transverse cross section is representative of the core−sheath structure along the full length of the fiber. Transmission electron microscopy (TEM) is inappropriate for many electrospun composite fibers since they are frequently too thick to be transparent to the electron beam.

Our approach to picture the internal morphology of the fibers is based on the use of FIB for cutting sections through the fiber in selected locations and along desired directions. This method is much more versatile, and it can be applied to any type of core−sheath fiber, including relatively soft fibers such as the PVP−liquid crystal composite fibers studied here. It should be a highly attractive tool also for characterizing other multicomponent fibers produced *via* coaxial electrospinning or other methods.[40,41] Importantly, the exact same sample can be characterized by other methods (here, optical microscopy) prior to FIB sectioning, hence we get complementary data from multiple techniques that allow a much richer description of the composite fiber. Previously, FIB milling on electrospun fibers was used only to image the cross section of simple, noncoaxially spun fibers without internal structure.[42]

When pumping the sheath solution at a flow rate of 1.8 mL $h^{-1}$, we achieve continuous fibers with encapsulated liquid crystal, where the flow rate of the latter can be varied between 0.1 and 0.9 mL $h^{-1}$. For low liquid crystal flow rates, fibers with smooth cylindrical morphology and outer diameter in the 1−2 $\mu$m range were obtained, but the filling was discontinuous, with the liquid crystal distributed in elongated droplets

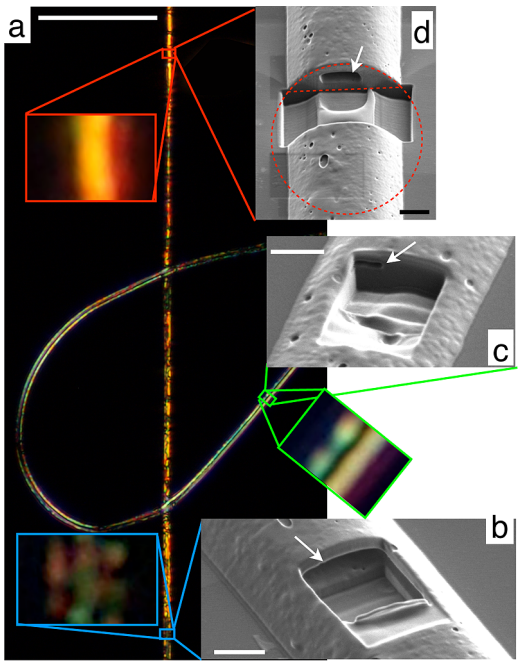


**Figure 1. (a) Reflection POM image of fibers spun with outer/inner flow rates of 1.8 and 0.20 mL $h^{-1}$, respectively. Three areas highlighted by rectangles are shown with 10 times lateral magnification in the three insets. (b−d) Internal morphology is revealed at the same three locations by FIB milling (30 pA current). The straight fiber was filled with liquid crystal, as proven by the relatively large cavities (indicated by white arrows) visible in (b) and (d), whereas the curved fiber was close to unfilled, with only a tiny cavity seen in (c). To emphasize the external horizontal cylinder segment morphology in (d), the border between polymer and silicon substrate has been highlighted with a red horizontal line and a circle is drawn that along its top segment is tangent to the outside fiber boundary. Scale bars in the POM and FIB images correspond to 50 and 1 $\mu$m, respectively.**

along the fibers.[27,43] By increasing the liquid crystal flow rate, quasi-continuous filling could be ensured; see for instance the fibers in Figure 1, produced with 0.2 mL $h^{-1}$ liquid crystal flow rate. The polarizing optical microscopy (POM) image in (a) shows a typical fiber (the straight one running top-down in the figure) that is almost continuously filled, as well as a curved fiber that is essentially without liquid crystal filling (this represents a minority of the sample as a whole).

The nanoscale imaging carried out after "dissecting" the fibers with FIB milling at selected locations revealed that the fibers produced under these conditions were not truly cylindrical, as initially expected. While they most likely had been cylindrical in flight, they collapsed into a quite flat horizontal cylinder segment after the sample was deposited on the silicon substrate (cf. Figure 1b−d). This is probably less an effect of the impact on the silicon substrate than of wetting of the latter by the polymer sheath while it still contained much solvent. A larger distance to the collector would allow a higher degree of solvent evaporation and thus most likely a more cylindrical shape, as would collection as free-hanging mats between

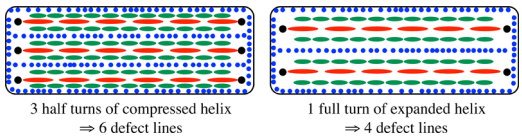


**Figure 2. Highly simplified illustration of the trade-off between helix distortion away from the natural pitch $p_0$ and the appearance of defect lines close to the side walls. Blue dots indicate director along the fiber (and the viewing direction), red lines director in the paper plane, perpendicular to the fiber. Large black dots symbolize defect lines running along the fiber. See main text for further explanation.**

split electrodes.[44] In some cases, such as for employing the fibers as lithographic etch/shadow masks,[45,46] the collapsed morphology with strong adhesion to the substrate is highly desirable.

**Cholesteric Liquid Crystal in Submicrometer Cavities.** The loss of cylindrical symmetry as the fibers collapsed onto the substrate led to interesting and sometimes unexpected variations of the shape of the core cavity in which the liquid crystal was contained. To expose its morphology, we excavated small rectangular sections within the fibers (Figure 1b,c) or we cut away complete slices (d). In (b), a wide inner channel is clearly visible, confirming the high degree of filling of the fiber by the liquid crystal. The channel here has an asymmetric shape with a relatively flat bottom and a curved upper boundary. Further up in (a) along the same fiber, the channel cross section is very different, with an essentially rectangular shape, as shown in (d).

The optical appearance of the straight fiber is inhomogeneous with relatively weak bicolored reflection from the area where the section shown in (b) was obtained. When confined in a space as narrow as this, between substrates imposing a unidirectional planar director orientation, the helix pitch, and thus the reflection color, is entirely determined by the confining geometry. This is because an integer number of half-pitches must fit between the bounding surfaces, yielding a quantization of the allowed colors.[17,27] For a cylindrical fiber with a fully circular cross section and inner diameter below 1 $\mu$m, the strict conditions of the cylindrical symmetry mean that the natural cholesteric pitch $p_0$ is almost unimportant. The reflection color is determined entirely by the cavity dimension, changing continuously from red to violet as the wall spacing decreases.[27] In the present less symmetric case, the confinement must be reduced to about 500 nm to obtain this extreme restricted situation. For the fibers in Figure 1, we can establish the cavity dimensions from the images obtained after FIB milling. Taking into account the imaging angle and measuring at the fiber center, we estimate the maximum vertical dimensions to be about 678 nm in (b) and 465 nm in (d), hence for this fiber, we are in the regime where the color is determined strongly or even fully by the confinement.

As described in the Supporting Information, we measured the natural helix pitch of our cholesteric to be about $p_0 = 310$ nm, while its average refractive index is about 1.5, giving it a blue natural color (air wavelength of the reflected light $\lambda_0 = 310 \times 1.5 = 465$ nm). Inside the fiber, the liquid crystal must generally either compress or expand the helix to comply with the boundary conditions, as just discussed. Considering first the nonrectangular cavity in (b), the helix must obviously develop from the flatter "floor" to the more curved "ceiling". At the highest point, the cavity can fit two pitches, slightly adjusted to be about 30 nm longer than $p_0$, hence this would be the pitch offset $\Delta p_e$ if the helix expands to fill the cavity with two complete turns. If it instead would compress to fit five half-turns, then the compressed pitch would be $p_c = 678/5 \times 2 = 271$ nm, giving an offset of about $\Delta p_c = -40$ nm. As the expansion gives the smallest elastic energy penalty, we can thus deduce that the selectively reflected light should have a wavelength around $\lambda_e = 339 \times 1.5 = 509$ nm in air, which corresponds to a green color. Indeed, looking at the optical zoom-in of the area in question, we see that the fiber looks green along the center.

Two rather thick defect lines border the green color on both sides, and toward the fiber edges, the color is more orange-red, at the same time as the colored appearance is very weak in some parts. Just like in a classic Cano wedge cell,[17] the decreasing distance between the cavity floor and ceiling as we approach the cavity edge should initially compress the helix. Eventually, the elastic distortion will, however, be smaller if the liquid crystal makes a smaller number of half-helix turns with an expanded pitch, and where this happens, the defect line develops. Because the cavity shape here is not that of a perfect arch, but flatter in the central region with a much more rapidly reducing height toward the sides (see Figure 4, obtained from the same fiber), it seems that the magnitude of the jump at the defect corresponds to multiple half-helix turns, leaving only one or two half-helices at the edges with a strongly expanded pitch. This explains the red-orange color seen along the fiber border in this section of the sample. The overall weak color in this section of the fiber indicates that the presence of the two defect lines and strong discontinuity in the helical arrangement have a strongly negative influence on the reflection efficiency.

In the regime where image (d) was obtained, the POM texture (a) appears much more uniform with a strong orange-red reflection color. The uniform optical appearance fits well with the rectangular shape of the cavity in (d), more similar to a standard flat sample cell. As in such a cell, the greater extension in the horizontal direction gives a vertically oriented helix. Considering only the vertical dimension, the somewhat smaller height compared to the maximum height in (b) would actually make a 3/2 turn helix with natural pitch the most favorable at this location. This would give rise to the natural blueish selective reflection color, yet the optical photo in (a) reveals a very different color in this

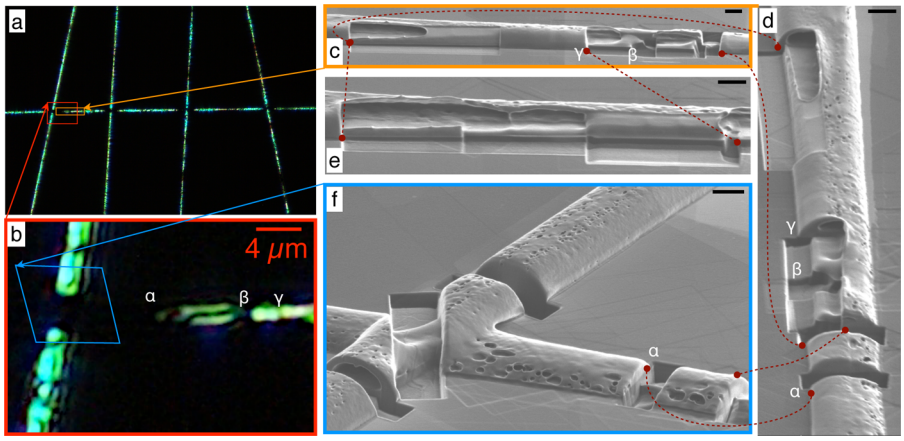


**Figure 3. (a,b) Reflection POM image of fibers spun with outer/inner flow rates 1.8 and 0.84 mL $h^{-1}$, respectively. Image (b) is a zoom-in of the red square in (a). (c,d) FIB images from two different angles of the fiber within the orange box in (a), after several cuts have been made through the fiber with FIB milling (30 pA). (e) FIB image of the fiber in (c,d) after more of the sheath top has been cut away using FIB milling. (f) FIB image of the fiber crossing point after several cuts have been made in each fiber and through the crossing point. Note that the imaging perspective in (c) and (e) is "from the top" of the (a,b) photos, hence the fiber orientation appears reversed in (c) and (e) compared to the optical images. In (d), the perspective is away from the cross, from left to right in (b). Greek letters identify locations common to the different images, and guidelines connect them between the different panes. Black scale bars in (c−f) represent 1 $\mu$m (only a guideline since the perspective imaging leads to a varying scale throughout the image). The irregularly distributed pits on the sheath are artifacts induced by the FIB during imaging.**

region. On the other hand, if we consider only one full turn developing with expanded pitch, we would obtain reflection centered around $\lambda = 465 \times 1.5 = 698$ nm. While a bulk sample with this pitch would give a distinctly red color, here, in order to explain the appearance, we must take the broadening of the reflection into account.[28] For samples as thin as this, the reflection window extends toward shorter visible wavelengths as well as into the infrared, rendering the shift toward an orange character understandable.

In order to understand the unexpected expansion of the pitch, we must now consider also the influence from the vertical walls (cf. Figure 2). Their presence in this extreme confinement constitutes a key difference from the standard liquid crystal sample, where the side area is only a tiny fraction of the top and bottom areas. The substrate distance is also 1−2 orders of magnitude greater in that case, hence any influence from the air bounding the liquid crystal along the sides is negligible. In the fiber cavity, in contrast, the vertical side length is more than one-third of the cavity width (which is about 1.3 $\mu$m), and the liquid crystal here is in contact with the same planar-aligning PVP as at the floor and ceiling. The director is aligned along the fiber also at these walls, an alignment that is incompatible with the helix running vertically in the middle part of the cell (see Figure 2). This means that a defect line must appear close to each wall once per every half-turn of the vertical helix, whenever the director in the bulk becomes perpendicular to the director at the wall. Obviously, an expansion of the helix reduces the number of defect lines, from six to four at this extremely small substrate separation, leading to a 33% decrease in the free energy cost from defects. It is nontrivial to estimate the exact energy density along a defect line of this type, but it must be expected to be quite high compared to the small elastic energy density related to helix compression/expansion (the twist elastic constant of a nematic or cholesteric is very small, on the order of 1 pN).[17] Moreover, while the latter energy cost due to compression/expansion scales with the channel volume, thus kept small in this very narrow channel, the former energy cost due to the disclinations at the wall is the same regardless of width, thus acquiring relevance with respect to the sample as a whole only in a channel as narrow as this one. This would explain why the liquid crystal chooses to expand the helix in a cavity of this shape and these dimensions, minimizing the number of defect lines from six to four at the cost of a helix pitch quite far from the natural value $p_0$, giving rise to the red-orange color.

In contrast to the overall colorful straight fiber in Figure 1a, the optical texture of the curved fiber is dominated by a dark core. The fiber is sporadically decorated with small colored spots, but these are overlaid with a bright background arising from birefringence from the polymer sheath, in which the PVP has been stretch-aligned during spinning (this contribution is not seen in the straight fiber since it is oriented such that the optic axis of the PVP is aligned along the polarizer). The general absence of cholesteric reflection color in this curved fiber suggests a much lower degree of liquid crystal filling, a conclusion that is confirmed by the inspection of the fiber cross section, shown in (c). The inner morphology is very different from that of the straight fiber imaged in (b) and (d), with only a tiny channel, seen as a small hole in the upper left corner in (c). Its height is about 160 nm, hence the liquid crystal can develop half a helix turn with only a slight expansion from the natural pitch. The

reflection wavelength would then be centered around 480 nm, corresponding to cyan. When overlaid with the birefringence color from the sheath, the result is the greenish spot that can be seen in the zoomed-in section.

It is remarkable that the reflection color can be detected even when only half a helix turn can fit in the cavity. This is a beautiful testament to the benefit of the continuous helical photonic structure formed by cholesteric liquid crystals. The periodicity is inherent to the spontaneous arrangement of the molecules on any scale. The photonic crystal properties thus remain for extremely thin samples, although of course with weak signal strength and considerable broadening of the spectral response.[28]

**Longitudinal Structure of the Cavities.** The images in Figure 1 suggest that the liquid crystal core channel is continuous over relatively long distances, but there may be interruptions and the channel cross section can be quite different from the external fiber morphology. Throughout the samples studied, the outer cross section is one of an almost perfect horizontal cylinder segment. To get a better picture of the variation of the internal channel morphology along a more richly filled fiber, we conducted a series of investigations on another sample, spun with higher liquid crystal flow rate (cf. Figure 3).

The higher core fluid flow rate ensured that the fibers were almost completely filled, and it also led to wider fibers with more uniform and on average somewhat larger cavities. The fiber color was quite uniform in the blue-green range. The FIB investigation revealed a core channel that generally had a clearly arched shape, with flatter bottom and more uniformly curved top than in the imperfect arch-like channel fiber discussed above. In analogy with that fiber, we should see a different color along the center and along the edges. This is in fact what we observe, but the defect line is much less apparent and the difference in color is now more subtle, with a blue center and blueish-green sides. The difference is most likely an effect of the smoother cavity shape here allowing a jump of only half a helix at the defect line. A quantitative analysis of the image reveals a central height of 612 nm, fitting two full turns of the helix with only a minor compression of the pitch from $p_0$, giving the center a color very close to the natural one (306 × 1.5 = 459 nm). As the confinement gets narrower toward the side, the pitch decreases continuously and the helix becomes further compressed, yet this may be compensated to some extent by the helix direction curving within the fiber as a result of the top substrate curvature. When the substrate distance has decreased sufficiently, the pitch offset becomes smaller if only three half-turns of a slightly expanded helix develops. A calculation analogous to that above then yields the expanded pitch of about 355 nm, giving reflection at an air wavelength of about 530 nm, resulting in the green appearance seen along the fiber sides.

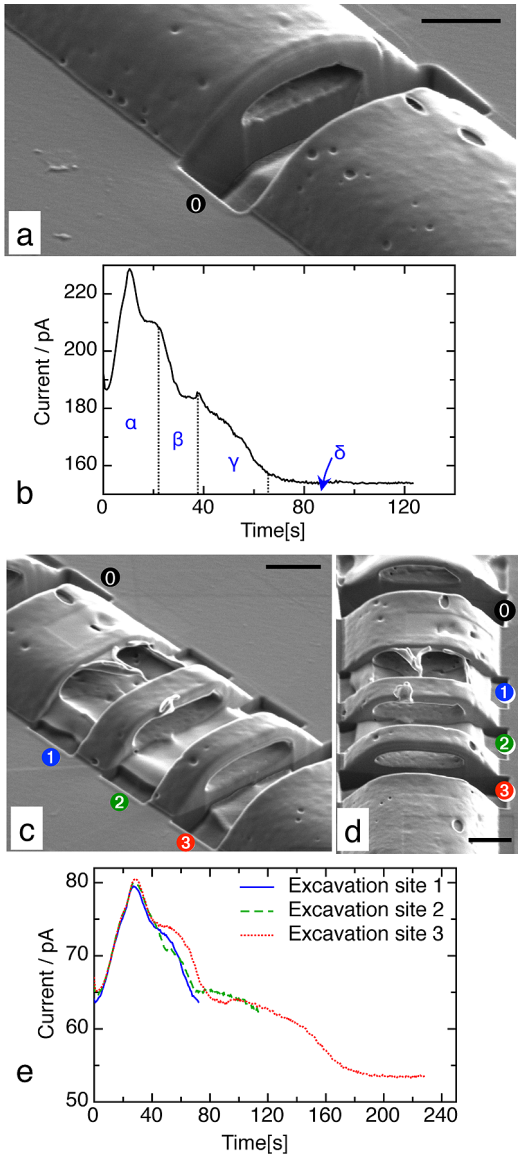


**Figure 4. (a) Originally well-filled fiber in which a perpendicular slice has been cut away by FIB milling (0.1 nA, 120 s). The end-point current during cutting (b) exhibits steps associated with different materials in the fiber. (c,d) Three adjacent cuts in the same fiber, at constant current (30 pA) but with milling times of 70, 120, and 220 s, respectively, yielding successively increasing excavation depth. Two perspectives are shown for better visualizing the different sections with shortest (1) to longest (3) exposure time. The corresponding end-point currents are shown in graph (e). Scale bars in the FIB images correspond to 1 $\mu$m.**

We cut several perpendicular slices through the fiber to expose the internal cross section, but we now also cut the fiber in the longitudinal direction to get a clear view of the continuity of the internal channel (cf. Figure 3c–e). The FIB milling reveals that the liquid crystal channel in the bottom fiber grew narrower on approaching any fiber crossing point, eventually leaving just pure polymer in the direct vicinity of the crossing (Figure 3d,f). At this point, the two crossing fibers have merged completely, providing a second piece of evidence that the polymer contained enough

solvent to be highly fluid when the fibers reached the substrate.

The absence of core fluid at all fiber crossing points in these collapsed fibers was easily recognized also in polarizing microscopy (Figure 3a,b) where the points of fiber crossing always appear entirely dark. This suggests that the pressure between the fibers "squeezes" the liquid crystal away from the crossing point. If total continuity of the core, also past fiber crossings, is important, as for instance in the case where a conducting fluid is encapsulated, it is thus important that the fiber sheath solidifies sufficiently in flight and gains a sufficient rigidity to counteract this flattening of the core when fibers cross. On the other hand, the merging of the fibers should provide a considerable enhancement of the mechanical strength of the fiber mat compared to a nonwoven where fibers are deposited on top of each other as separate entities. As seen in Figure 3b,f, the fibers can be filled almost up to the crossing point, hence this may in many cases be a useful compromise.

In the other direction, further from the cross (top of Figure 3d), the filling is quite rich and the liquid crystal has apparently expanded in the lateral direction, resulting in a fiber that is substantially wider and flatter than close to the crossing point. However, even the seemingly continuous channel further away from the crossing was in fact interrupted by thin polymer walls at some points, as exposed by longitudinal sectioning. Figure 3c,e shows the fiber at two stages of longitudinal excavation. In the final stage image (e), the channel has been largely laid open, and roughly in the middle of the revealed channel, a thin wall separating two compartments can be seen.

**Monitoring the Milling Process.** The current collected during the ion milling (end-point current, EPC) is material-dependent and can thus be used to identify different layers in a heterogeneous structure. An increase or decrease in the milling current indicates that an interface has been encountered.[47] The current thus provides a valuable source of information for us, allowing to control the excavation quite precisely by monitoring the current in real time. When excavating a properly filled fiber (same sample as in Figure 1), as shown in Figure 4a (image of the dissected fiber, which has a well-developed channel that was hosting liquid crystal prior to dissection), the current profile showed distinct step-like behavior, as shown in Figure 4b. The hemicylindrical geometry of our coaxial fibers with a fluid core renders the analysis in terms of multilayer structure more complex than for a flat multilayered composite, but we can nevertheless clearly identify four different regimes in the current response. These correspond to the encounter of the outer polymeric surface of the fiber (region $\alpha$ in Figure 4b), the complete removal of the top sheath, and the breakthrough into the liquid crystal core (region $\beta$), the removal of the bottom part of the polymer sheath (region $\gamma$), and finally the silicon substrate (region $\delta$).

The correspondence between the regions in the EPC graph and the different parts of the fiber was confirmed by performing a series of adjacent cuts along the same fiber with different milling times (cf. Figure 4c–e). In order to have a finer control of the milling process, these excavations were realized with a FIB current of 30 pA, lower than the current of 0.1 nA used during the experiment reported in Figure 4a. The milling times were based on the times when the current changed in graph (b), scaled in accordance with the reduced current. In this way, we aimed to remove selectively different portions of the fiber: the top polymeric shell (cut 1; 70 s), all the polymer defining the cavity (cut 2; 120 s), and the complete fiber (cut 3; 220 s). In Figure 4c,d, we report images of the fiber after the systematic cuts with the numbers identifying the different sites. The corresponding currents are shown in the graph in Figure 4e.

## CONCLUSIONS

We have demonstrated that cholesteric liquid crystals exhibit selective reflection also when confined in a space much smaller than a micrometer, such that only a few or even just one-half turn of the helix can form. At this small scale, tiny variations in dimension and shape give strong changes in the reflected color. This correlation between optical properties and submicrometer cavity morphology was made possible by combining FIB milling with polarizing optical microscopy. Further studies should aim to obtain a quantitative correlation between the spectral response and the shapes and dimensions of each cavity. The ability to cut away sections of any size and in any direction from the fibers using the FIB gives us a picture of the core–sheath structure with unprecedented detail. The strategy should be extremely useful for characterizing also many other types of composite fibers produced by coaxial electrospinning or other fabrication methods.

## METHODS

As sheath solution, a mixture of 12.5 wt % PVP (MW 1 300 000 g/mol, Acros) and 0.5 wt % NaCl (added to increase the conductivity and thus aid the electrospinning process) in ethanol was used. The chiral liquid crystal was a 50:50 mixture (by weight) of the chiral dopant (*S*)-4-cyano-4-(2-methylbutyl)biphenyl (Synthon Chemicals) and the nematic mixture RO-TN-403/015S (Hoffmann-La Roche). The fibers were produced at room temperature where this mixture shows a short-pitch cholesteric phase giving rise to intense blue reflection. Also, the optical microscopy investigations were carried out at room temperature.

In the electrospinning experiment, the polymer solution was pumped through a metallic tube while the liquid crystal was pumped through a flexible capillary inserted coaxially into the

former (see refs 27 and 29 for details). The flow rates were adjusted by a microfluidics control unit (Fluigent MFCS-4C). An electric voltage of 10 kV was applied by a high-voltage power supply (Gamma High Voltage Research) attached to the metallic tube and a grounded aluminum foil. This was placed 10 cm below the tube and served as collector. The fibers were spun onto silicon substrates placed onto the collector.

During FIB investigations, the fibers were irradiated with 30 kV $Ga^+$ ions using a dual-beam FIB system (FEI QUANTA 200 3D). The excavations are made by fixing the ion current at 0.1 nA or 30 pA and changing the milling time for controlling the depth. After milling, the fiber was imaged by the same FIB system, using substantially lower acceleration voltage. Unfortunately, the ion beam still acts destructively on the polymer sheath (which was not coated by any protective metal but imaged directly), leading to irregularly distributed small pits along the fiber. These pits are thus artifacts generated from the FIB imaging technique and do not reflect the pristine fiber. Polarizing microscopy images were obtained with a Nikon Eclipse microscope operating in reflection mode.

*Conflict of Interest:* The authors declare no competing financial interest.

*Acknowledgment.* We thank Jan Lagerwall for help in the preparation of the fibers and for fruitful discussions, and JungHyun Noh for assistance in measuring the natural pitch of the cholesteric liquid crystal mixture. Financial support from the National Research Foundation (NRF), Korea, Grant Number 490-20120011, is gratefully acknowledged.

*Supporting Information Available:* Determination of the average refractive index *via* the natural cholesteric helix pitch. This material is available free of charge *via* the Internet at http://pubs.acs.org.

## REFERENCES AND NOTES

1. Hess, O.; Pendry, J.; Maier, S.; Oulton, R.; Hamm, J.; Tsakmakidis, K. Active Nanoplasmonic Metamaterials. *Nat. Mater.* **2012**, *11*, 573–584.
2. Litchinitser, N. Structured Light Meets Structured Matter. *Science* **2012**, *337*, 1054–1055.
3. Zheludev, N. I.; Kivshar, Y. S. From Metamaterials to Metadevices. *Nat. Mater.* **2012**, *11*, 917–924.
4. Forster, J. D.; Park, J.-G.; Mittal, M.; Noh, H.; Schreck, C. F.; O'Hern, C. S.; Cao, H.; Furst, E. M.; Dufresne, E. R. Assembly of Optical-Scale Dumbbells into Dense Photonic Crystals. *ACS Nano* **2011**, *5*, 6695–6700.
5. Lagerwall, J. P. F.; Scalia, G. A New Era for Liquid Crystal Research: Applications of Liquid Crystals in Soft Matter Nano-, Bio- and Microtechnology. *Curr. Appl. Phys.* **2012**, *12*, 1387–1412.
6. Zografopoulos, D. C.; Asquini, R.; Kriezis, E. E.; d'Alessandro, A.; Beccherelli, R. Guided-Wave Liquid-Crystal Photonics. *Lab Chip* **2012**, *12*, 3598–3610.
7. De Sio, L.; Ferjani, S.; Strangi, G.; Umeton, C.; Bartolino, R. Universal Soft Matter Template for Photonic Applications. *Soft Matter* **2011**, *7*, 3739–3743.
8. Lorenz, A.; Schuhmann, R.; Kitzerow, H.-S. Infiltrated Photonic Crystal Fiber: Experiments and Liquid Crystal Scattering Model. *Opt. Express* **2010**, *18*, 3519–3530.
9. Kim, H.; Ge, J.; Kim, J.; Choi, S.; Lee, H.; Lee, H.; Park, W.; Yin, Y.; Kwon, S. Structural Colour Printing Using a Magnetically Tunable and Lithographically Fixable Photonic Crystal. *Nat. Photonics* **2009**, *3*, 534–540.
10. Fontana, J.; Bailey, C.; Weissflog, W.; Janossy, I.; Jakli, A. Optical Waveguiding in Bent-Core Liquid-Crystal Filaments. *Phys. Rev. E* **2009**, *80*, 032701.
11. Cuennet, J. G.; Vasdekis, A. E.; De Sio, L.; Psaltis, D. Optofluidic Modulator Based on Peristaltic Nematogen Microflows. *Nat. Photonics* **2011**, *5*, 234–238.
12. O'Neill, M.; Kelly, S. Ordered Materials for Organic Electronics and Photonics. *Adv. Mater.* **2011**, *23*, 566–584.
13. Coles, H.; Morris, S. Liquid-Crystal Lasers. *Nat. Photonics* **2010**, *4*, 676–685.
14. Humar, M.; Ravnik, M.; Pajk, S.; Musevic, I. Electrically Tunable Liquid Crystal Optical Microresonators. *Nat. Photonics* **2009**, *3*, 595–600.
15. Woltman, S.; Jay, G.; Crawford, G. Liquid-Crystal Materials Find a New Order in Biomedical Applications. *Nat. Mater.* **2007**, *6*, 929–938.
16. Mitov, M.; Dessaud, N. Going beyond the Reflectance Limit of Cholesteric Liquid Crystals. *Nat. Mater.* **2006**, *5*, 361–364.
17. de Gennes, P.-G.; Prost, J. *The Physics of Liquid Crystals*; Clarendon Press: Oxford, UK, 1993.
18. Li, Q.; Li, Y.; Ma, J.; Yang, D.; White, T.; Bunning, T. Directing Dynamic Control of Red, Green, and Blue Reflection Enabled by a Light-Driven Self-Organized Helical Superstructure. *Adv. Mater.* **2011**, *23*, 5069–5073.
19. Han, Y.; Pacheco, K.; Bastiaansen, C. W. M.; Broer, D. J.; Sijbesma, R. P. Optical Monitoring of Gases with Cholesteric Liquid Crystals. *J. Am. Chem. Soc.* **2010**, *132*, 2961–2967.
20. Humar, M.; Musevic, I. 3D Microlasers from Self-Assembled Cholesteric Liquid-Crystal Microdroplets. *Opt. Express* **2010**, *18*, 26995–27003.
21. Russell, P. Photonic Crystal Fibers. *Science* **2003**, *299*, 358–362.
22. Mertens, G.; Wehrspohn, R. B.; Kitzerow, H.-S.; Matthias, S.; Jamois, C.; Gösele, U. Tunable Defect Mode in a Three-Dimensional Photonic Crystal. *Appl. Phys. Lett.* **2005**, *87*, 241108.
23. Takeda, H.; Yoshino, K. Tunable Light Propagation in Y-Shaped Waveguides in Two-Dimensional Photonic Crystals Utilizing Liquid Crystals as Linear Defects. *Phys. Rev. B* **2003**, *67*, 073106.
24. Ondris-Crawford, R.; Ambrozic, M.; Doane, J.; Zumer, S. Pitch-Induced Transition of Chiral Nematic Liquid Crystals in Submicrometer Cylindrical Cavities. *Phys. Rev. E* **1994**, *50*, 4773.
25. Kitzerow, H.; Liu, B.; Xu, F.; Crooker, P. Effect of Chirality on Liquid Crystals in Capillary Tubes with Parallel and Perpendicular Anchoring. *Phys. Rev. E* **1996**, *54*, 568–575.
26. Matthias, H.; Schweizer, S.; Wehrspohn, R.; Kitzerow, H. S. Liquid Crystal Director Fields in Micropores of Photonic Crystals. *J. Opt. A: Pure Appl. Opt.* **2007**, *9*, S389–S395.
27. Enz, E.; Lagerwall, J. Electrospun Microfibres with Temperature Sensitive Iridescence from Encapsulated Cholesteric Liquid Crystal. *J. Mater. Chem.* **2010**, *20*, 6866–6872.
28. John, W. S.; Fritz, W.; Lu, Z.; Yang, D.-K. Bragg Reflection From Cholesteric Liquid Crystals. *Phys. Rev. E* **1995**, *51*, 1191.
29. Enz, E.; Baumeister, U.; Lagerwall, J. Coaxial Electrospinning of Liquid Crystal-Containing Poly(vinyl pyrrolidone) Microfibers. *Beilstein J. Org. Chem.* **2009**, *5*, 5.
30. Lagerwall, J. P. F.; McCann, J. T.; Formo, E.; Scalia, G.; Xia, Y. Coaxial Electrospinning of Microfibres with Liquid Crystal in the Core. *Chem. Commun.* **2008**, *42*, 5420–5422.
31. Buyuktanir, E. A.; Frey, M. W.; West, J. L. Self-Assembled, Optically Responsive Nematic Liquid Crystal/Polymer Core–Shell Fibers: Formation and Characterization. *Polymer* **2010**, *51*, 4823–4830.
32. Yarin, A. Coaxial Electrospinning and Emulsion Electrospinning of Core–Shell Fibers. *Polym. Adv. Technol.* **2011**, *22*, 310–317.
33. Yuan, T.; Zhao, B.; Cai, R.; Zhou, Y.; Shao, Z. Electrospinning Based Fabrication and Performance Improvement of Film Electrodes for Lithium-Ion Batteries Composed of $TiO_2$ Hollow Fibers. *J. Mater. Chem.* **2011**, *21*, 15041–15048.
34. Chen, H.; Wang, N.; Di, J.; Zhao, Y.; Song, Y.; Jiang, L. Nanowire-in-Microtube Structured Core/Shell Fibers *via* Multifluidic Coaxial Electrospinning. *Langmuir* **2010**, *26*, 11291–11296.
35. Miyauchi, M.; Miao, J.; Simmons, T.; Lee, J.; Doherty, T.; Dordick, J.; Linhardt, R. Conductive Cable Fibers with Insulating Surface Prepared by Coaxial Electrospinning of Multiwalled Nanotubes and Cellulose. *Biomacromolecules* **2010**, *11*, 2440–2445.
36. Zhao, Y.; Cao, X.; Jiang, L. Bio-Mimic Multichannel Microtubes by a Facile Method. *J. Am. Chem. Soc.* **2007**, *129*, 764–765.

37. Yang, H.; Lightner, C.; Dong, L. Light-Emitting Coaxial Nanofibers. *ACS Nano* **2012**, *6*, 622–628.
38. Kwak, G.; Lee, G.; Shim, S.; Yoon, K. Fabrication of Light-Guiding Core/Sheath Fibers By Coaxial Electrospinning. *Macromol. Rapid Commun.* **2008**, *29*, 815–820.
39. Li, D.; Xia, Y. Direct Fabrication of Composite and Ceramic Hollow Nanofibers by Electrospinning. *Nano Lett.* **2004**, *4*, 933–938.
40. Wu, W.; Bai, S.; Yuan, M.; Qin, Y.; Wang, Z. L.; Jing, T. Lead Zirconate Titanate Nanowire Textile Nanogenerator for Wearable Energy-Harvesting and Self-Powered Devices. *ACS Nano* **2012**, *6*, 6231–6235.
41. Xie, J.; MacEwan, M.; Schwartz, A.; Xia, Y. Electrospun Nanofibers for Neural Tissue Engineering. *Nanoscale* **2010**, *2*, 35–44.
42. Liu, H.; Edel, J.; Bellan, L.; Craighead, H. Electrospun Polymer Nanofibers as Subwavelength Optical Waveguides Incorporating Quantum Dots. *Small* **2006**, *2*, 495–499.
43. Scalia, G.; Enz, E.; Calò, O.; Kim, D. K.; Hwang, M.; Lee, J. H.; Lagerwall, J. P. F. Morphology and Core Continuity of Liquid-Crystal-Functionalized, Coaxially Electrospun Fiber Mats Tuned *via* the Polymer Sheath Solution. *Macromol. Mater. Eng.* **2013**, *298*, 583–589.
44. Dersch, R.; Liu, T.; Schaper, A.; Greiner, A.; Wendorff, J. Electrospun Nanofibers: Internal Structure and Intrinsic Orientation. *J. Polym. Sci., Part A* **2003**, *41*, 545–553.
45. Ishii, Y.; Sakai, H.; Murata, H. Fabrication of a Submicron-Channel Organic Field-Effect Transistor Using a Controllable Electrospun Single Fibre as a Shadow Mask. *Nanotechnology* **2011**, *22*, 205202.
46. Czaplewski, D.; Kameoka, J.; Craighead, H. Nonlithographic Approach to Nanostructure Fabrication Using a Scanned Electrospinning Source. *J. Vac. Sci. Technol., B* **2003**, *21*, 2994–2997.
47. Reyntjens, S.; Puers, R. A Review of Focused Ion Beam Applications in Microsystem Technology. *J. Micromech. Microeng.* **2001**, *11*, 287–300.